Decoherence scaling transition in the dynamics of quantum information scrambling

Federico D. Domínguez,[1,*] María Cristina Rodríguez,[1,2] Robin Kaiser,[3] Dieter Suter,[4] and Gonzalo A. Álvarez[1,2,5,†]

[1]*Centro Atómico Bariloche, CONICET, CNEA, S. C. de Bariloche, Argentina.*
[2]*Instituto Balseiro, CNEA, Universidad Nacional de Cuyo, S. C. de Bariloche, Argentina.*
[3]*Institut Non-Linéaire de Nice, CNRS, Université de Nice Sophia Antipolis, 06560, Valbonne, France.*
[4]*Fakultät Physik, Technische Universität Dortmund, D-44221, Dortmund, Germany.*
[5]*Instituto de Nanociencia y Nanotecnologia, Departamento de Física Médica, CNEA, CONICET, S. C. de Bariloche, 8400, Argentina*

Reliable processing of quantum information for developing quantum technologies requires precise control of out-of-equilibrium many-body systems. This is a highly challenging task as the fragility of quantum states to external perturbations increases with the system-size. Here, we report on a series of experimental quantum simulations that allow to quantify the sensitivity of a controlled Hamiltonian evolution to perturbations that drive the system away from the targeted evolution. Based on out-of-time order correlations, we demonstrate that the decay-rate of the process fidelity increases with the effective number K of correlated qubits as K^{α}. As a function of the perturbation strength, we observed a sharp decoherence scaling transition of the exponent α between two distinct dynamical regimes. In the limiting case below the critical perturbation strength, there is not inherent limit to the number of qubits that can be controlled with high fidelity. This may indicate that reliable control of large quantum systems might be possible if the perturbation can be kept below this critical threshold.

The characterization and understanding of the complex dynamics of interacting many-body quantum systems is an outstanding problem in physics [1, 2]. They play a crucial role in condensed matter physics, cosmology, quantum information processing and nuclear physics [3, 4]. A particularly urgent issue is the reliable control of many-body quantum systems, as it is perhaps the most important step towards the development and deployment of quantum technologies [1, 5–7]. Their control is never perfect and the fragility of quantum states to perturbations increases with the system size [8–10]. Accordingly, information processing with large quantum systems remains a challenging task. It is therefore of paramount importance to reduce the sensitivity to perturbations, particularly for large systems, to minimize the loss of quantum information. As we show here, achieving this goal may be more realistic than it is currently assumed: we demonstrate for the first time that the sensitivity of a quantum system to environmental noise can become qualitatively smaller, if the control operations applied to it surpass a certain threshold.

The degrading of quantum information due to environmental noise is generally known as decoherence. Mitigating this effect has been the goal of numerous studies to allow information storage by protecting quantum states [10]. However, characterizing and controlling decoherence effects during the dynamics of quantum information remain challenging tasks, since out-of-equilibrium many-body physics is involved [4, 5, 11, 12]. Theoretical and experimental approaches were developed to reduce decoherence in few-body systems [10, 13]. Extending these approaches to larger quantum systems is not a straightforward scaling operation, since the evolution in these systems generates high-order quantum correlations that are spread over degrees of freedom of many qubits. Controlling and probing these correlations was tackled only recently [12, 14–16]. Novel techniques are therefore required to address this task, in particular with quantum simulations [5, 6, 9, 17, 18].

The dynamics of the build-up of many-body quantum superpositions was initially measured within nuclear magnetic resonance (NMR) by observing multiple quantum coherences (MQC) [19]. MQCs are relatively easy to characterize and the order of the coherence provides a hard lower bound on the number of correlated particles (spins) [4, 9, 20, 21]. Combined with time-reversal of quantum evolutions leading to a Loschmidt echo [22, 23], they are useful tools to measure the sensitivity of controlled dynamics to perturbations. Loschmidt echoes and MQC evidence out-of-time order correlations (OTOC) [3, 4], as they measure the scrambling of the information over a large system from an initially localized state [20, 21, 24]. They are therefore promising tools for finding answers to open questions related to quantum chaos [25–27], irreversibility [24, 28], thermalization [29] and entanglement [21]. Hence, these OTOCs trigger a broad interest in diverse fields of physics, such as condensed matter and quantum gravity, opening new avenues for understanding the dynamics of quantum information in complex systems [3, 4].

Here, we use the tools of solid-state NMR to assess the sensitivity to perturbations of a controlled quantum dynamics in a many-body system. We drive the system away from equilibrium by suddenly imposing on it an experimentally controllable Hamiltonian that does not commute with the initial condition and that can be inverted, in order to drive the system forward or backward in time. The forward motion causes the quantum information to spread over a large system (with thousands of particles), but in the case where the inversion of the Hamiltonian is perfect, the

system returns exactly to the initial state –this is known as a Loschmidt Echo [22, 23].

In practice, the inversion of the Hamiltonian is never perfect, and the deviations result in imperfect return to the initial condition and therefore to a reduction of the echo signal, which is proportional to the overlap between the initial and final state. Here, we study the effect of such deviations from the ideal Hamiltonian by adding perturbations with variable strength p and measuring their effect on the evolution. This sets a paradigmatic model system where initial information stored on local states spreads over a spin-network of about 5000 spins. This information spreading process is called scrambling [3, 4, 25], to indicate that the local initial condition can no longer be accessed by local measurements. We experimentally design an OTOC measure to probe high order quantum correlations and compare the scrambling of information from the initial state by the ideal and the perturbed quantum dynamics. This is done by implementing a Loschmidt echo with a forward evolution driven by the perturbed Hamiltonian and a backward evolution driven by the ideal one, so as we quantify the difference between the scrambling dynamics. This OTOC defines an effective cluster size, the number of correlated spins K over which the information was spread by the ideal control Hamiltonian. We demonstrate that the fidelity decay rate of the controlled dynamics –measured with the Loschmidt Echo– increases with the instantaneous cluster-size K, as a power law $\propto K^{\alpha}$, with α depending on the perturbation strength p. Strikingly, our results evidence two qualitatively different fidelity decay regimes with different scaling laws associated with a sudden change of the exponent α. For perturbations larger than a given threshold, the controlled dynamics is localized, as manifested by a saturation of the cluster-size growth $K(t)$. This therefore imposes a limit on the number of qubits that can be controlled during a quantum operation. However, for perturbations lower than the threshold, the cluster-size K grows indefinitely and the exponent α drops abruptly, making the quantum dynamics of large systems qualitatively more robust against the perturbation. This sudden sensitivity reduction to perturbations is a promising quantum feature that may be used to implement reliable quantum information processing with many-body systems for novel quantum technologies.

We perform all quantum simulations on a Bruker Avance III HD 9.4T WB NMR spectrometer with a ^{1}H resonance frequency of $\omega_z = 400.15$ MHz. We consider the spins of the Hydrogen nuclei of polycrystalline adamantane, where the strength of the average dipolar interaction can be determined from the full-width-half-maximum of the resonance line 13 kHz. They constitute an interacting many-body system of equivalent spins $I = 1/2$ in a strong magnetic field. In the rotating frame of reference, the Hamiltonian reduces to

$$\mathcal{H}_{dd} = \sum_{i<j} d_{ij} \left[2I_z^i I_z^j - (I_x^i I_x^j + I_y^i I_y^j)\right], \qquad (1)$$

where I_x^i, I_y^i and I_z^i are the spin operators and d_{ij} the spin-spin coupling strengths that scale with the distance between spins $\propto 1/r_{ij}^3$. The dipolar interaction $\mathcal{H}_{dd}$ is truncated to the part that commutes with the stronger Zeeman interaction ($\omega_z \gg d_{ij}$), as the effects of the non-commuting part are negligible.

The quantum simulations start from the high-temperature thermal equilibrium state $\rho(0) \approx \left(\mathbb{I} + \frac{\hbar\omega_z}{k_B T} I_z\right)/\mathrm{tr}\{\mathbb{I}\}$, where $I_z = \sum_i I_z^i$ [30]. The unity operator $\mathbb{I}$ does not contribute to an observable signal, therefore $\rho(0) \propto I_z$ and it commutes with the hamiltonian $\mathcal{H}_{dd}$. In this state, the spins are uncorrelated and form the ensemble of local states that we consider as the initial local information.

To spread the local information, we drive the system out of equilibrium with the evolution operator $U_0(t) = e^{-it\mathcal{H}_0}$, with the double-quantum Hamiltonian

$$\mathcal{H}_0 = -\sum_{i<j} d_{ij} \left[I_x^i I_x^j - I_y^i I_y^j\right] \qquad (2)$$

as the ideal –non-perturbed– Hamiltonian. This Hamiltonian flips simultaneously two spins with the same orientation. Accordingly, the z-component of the magnetization M_z changes by $M = \Delta M_z = \pm 2$. At the same time, the number of correlated spins K changes by $\Delta K = \pm 1$. The coherence order $M = M_{z,j} - M_{z,i}$, classifies the coherence $|M_{z,i}\rangle\langle M_{z,j}|$ of the density matrix, where $I_z |M_{z,i}\rangle = M_{z,i} |M_{z,i}\rangle$. The change of coherence order allows to probe high-order spin correlations associated with the number of correlated spins that witness the information spreading over the system from the initial ensemble of localized states [19] (see Material and Methods).

To quantify the sensitivity to perturbations of the controlled quantum dynamics, we control the deviation from $\mathcal{H}_0$ with the dimensionless perturbation strength p of the hamiltonian

$$\mathcal{H} = (1-p)\mathcal{H}_0 + p\Sigma. \qquad (3)$$

Here Σ is a perturbation hamiltonian. The Hamiltonian $\mathcal{H}$ is engineered with average Hamiltonian techniques using a NMR pulse sequence [9] (see Material and Methods). We consider the effect of two different perturbations: i) a two spin operator perturbation given by the dipolar hamiltonian $\Sigma = \mathcal{H}_{dd}$ and ii) a single spin operator perturbation given by a longitudinal offset field $\Sigma = \mathcal{H}_z = \Delta\omega_z I_z$. The first case introduces a perturbation induced by spin-spin interactions, and the second case a relative dephasing with respect to the ideal evolution.

We quantify the deviation between the actual driven state $\rho(t) = I_z(t) = U(t) I_z U^\dagger(t)$ and the ideally driven state $\rho_0(t) = I_z^0(t) = U_0(t) I_z U_0^\dagger(t)$, where $U(t) = e^{-it\mathcal{H}}$ is the perturbed operation and $U_0(t) = e^{-it\mathcal{H}_0}$ the ideal control operation. The instantaneous state fidelity after a proper normalization is

$$f(t) = \langle \rho(t)\rho_0(t)\rangle = \left\langle I_z(t) I_z^0(t)\right\rangle, \qquad (4)$$

where $\langle\cdot\rangle = \mathrm{tr}\,[\cdot]$ (see Material and Methods). This fidelity is the projection between $\rho(t)$ and $\rho_0(t)$ and it is identical to the Loschmidt Echo [22, 23].

By choosing the observable I_z equal to the initial condition $\rho(0) = I_z$, we first evolve the system with the perturbed evolution operator $U(t)$ and then we time-reverse the evolution with the unperturbed evolution operator $U_0^\dagger(t)$ (see Material and Methods). This leads to the many-body Loschmidt-Echo $f(t) = \left\langle U_0^\dagger U I_z U^\dagger U_0 \cdot I_z \right\rangle$ that is equal to the fidelity after considering cyclic permutations.

We perform a partial tomography of the density matrix fidelity by applying a rotation operation $\phi_z = e^{i\phi I_z}$ between the forward $U(t)$ and backward evolution $U_0^\dagger(t)$. The global fidelity becomes

$$\begin{aligned} f_\phi(t) &= \left\langle U_0^\dagger \phi_z U I_z U^\dagger \phi_z^\dagger U_0 \cdot I_z \right\rangle \\ &= \left\langle I_z(t)\phi_z^\dagger I_z^0(t)\phi_z \right\rangle = \textstyle\sum_M e^{i\phi M} f_M(t), \end{aligned} \quad (5)$$

where we decompose it into the partial MQC-fidelities $f_M(t) = \langle \rho_M(t)\rho_{0,M}(t)\rangle$ of different coherence orders M, after a proper normalization (see Material and Methods).

If the perturbation strength $p = 0$, Equation (5) gives a conventional OTOC $f_\phi^0(t) = \left\langle I_z^0(t)\phi_z^\dagger I_z^0(t)\phi_z \right\rangle = \left\langle \phi_z(t) I_z \phi_z^\dagger(t) I_z \right\rangle$, with $\phi_z(t) = U_0^\dagger(t)\phi_z U^\dagger(t)$. Here $\langle\cdot\rangle$ is a expectation value if the system is assumed at infinite temperature (see Material and Methods). It quantifies the scrambling into the system of the initial information stored in the initial state I_z [4, 20]. The components $f_M^0(t) = \langle \rho_{0,M}(t)\rho_{0,M}(t)\rangle$ are the amplitudes of the MQC spectrum representing the distribution of coherences (non-diagonal terms in the eigenbasis of I_z) of the density matrix built-up by the control Hamiltonian $\mathcal{H}_0$ [9, 19]. The second-moment of $f_M^0(t)$ provides the average cluster-size of correlated spins $K_0(t)/2 = \frac{\sum_M M^2 f_M^0(t)}{\sum_M f_M^0(t)} = \left\langle [I_z^0(t), I_z]^\dagger [I_z^0(t), I_z] \right\rangle / \left\langle I_z^0(t) I_z^0(t) \right\rangle$ at the evolution time t [9, 19–21] (see Material and Methods). The expression $\left\langle [I_z^0(t), I_z]^\dagger [I_z^0(t), I_z] \right\rangle$ is a commutator OTOC quantifying the degree by which the initially commuting operators $I_z^0(t)$ and I_z fail to commute at time t due to the scrambling of information induced by the spin-spin interactions of $\mathcal{H}_0$ [20, 21].

Considering the perturbed evolution ($p \neq 0$), the fidelity $f_\phi(t)$ is a more general OTOC that quantifies the deviation of the scrambling induced by $\mathcal{H}$ with respect to the one driven by $\mathcal{H}_0$. This is seen from the second moment of $f_M(t)$,

$$\frac{K(t)}{2} = \frac{\sum_M M^2 f_M(t)}{\sum_M f_M(t)} = \frac{\left\langle [I_z(t), I_z]^\dagger [I_z^0(t), I_z] \right\rangle}{\left\langle I_z(t) I_z^0(t) \right\rangle}, \quad (6)$$

that based on the scalar product $\langle\cdot\rangle$ metric gives the degree of non-commutation shared by the evolved states $I_z^0(t)$ and $I_z(t)$ with respect to I_z (see Material and Methods). As $\mathcal{H}_{dd}$ and $\mathcal{H}_z$ do not generate MQC by themselves, this OTOC provides the scrambling of information by the spin-spin interactions of $\mathcal{H}_0$ that survived the perturbation effects. Based on the second moment of $f_M(t)$, $K(t)$ defines a "coherence length" between the two scrambling dynamics of information in terms of an *average hamming weight* [27, 29] for the fidelity of the density matrix. Therefore $K(t)$ quantifies how comparable the perturbed and unperturbed density matrix dynamics are as a function of the coherence order M. This coherence length $K(t)$ defines the effective cluster-size of correlated spins on which the density matrices are comparable based on the MQC fidelity $f_M(t) = \langle \rho_M(t)\rho_{0,M}(t)\rangle$ in Eq. (6).

We measure the time evolution of the MQC-fidelities $f_M(t)$ for different perturbations to determine the global fidelity $f(t)$ and the effective cluster-size $K(t)$. Both are shown in Fig. 1**A** and **B**, respectively, for a weak ($p = 0.0009$) and a strong perturbation strength ($p = 0.108$) when $\Sigma = \mathcal{H}_{dd}$. The fidelity decays faster as a function of time with increasing perturbation strength. The cluster-size $K(t)$ initially grows exponentially as a function of time and then slows down to a power law whose growth-rate reduces with increasing perturbation strength. For strong perturbations $K(t)$ saturates to a value independent of time that decreases with increasing perturbation strength [9]. We call this effect localization of the "coherence length" of the MQC-fidelity that quantifies the "localization" of the shared scrambling of information between the perturbed and ideal dynamics based on the OTOC of Eq. (6). The fidelity $f(t)$ reaches an exponential decay regimen with a constant rate when the dynamics of $K(t)$ is localized (Fig. 1**A**). Analogous results are observed for $\Sigma = \mathcal{H}_z$.

The fidelity decay $f(p,t) = e^{-\chi(p,t)}$ is determined by the instantaneous decoherence rate $\chi'(p,t) = \frac{d\chi}{dt}(p,t)$ (Fig. 1**C**). For strong perturbations, the decoherence rate $\chi'(t)$ reaches a plateau –a constant value– that depends on the perturbation strength when the dynamics of $K(t)$ is localized. However, for weak perturbations when the dynamics of $K(t)$ does not evidence localization, this plateau is not manifested. Consistently when localization effects are observed, $\chi'(K)$ evidences an accumulation of points as shown in Fig. 1**D**. This demonstrates that the saturation of $\chi'(t)$ and $K(t)$ occurs at the same time. Moreover, the experimental results shows that $\chi'(K) \propto K^\alpha$ for long times, indicating that the fidelity decay rate is determined by a scrambling rate defined by the instantaneous effective cluster-size K of correlated spins.

Figure 2 shows χ' as a function of K, now for both perturbation Hamiltonians $\Sigma = \mathcal{H}_{dd}$ and $\Sigma = \mathcal{H}_z$ and different perturbation strengths. The power law functional form $\chi'(K) \sim K^\alpha$ holds for all the considered cases. The exponents α are shown in Fig. 2**C**. They give qualitative different limiting values for the localized (strong perturbation) and delocalized curves (weak perturbation). For the strongest perturbations, the asymptotic behavior at long times shows a power law $\chi'(K) \sim K^{\alpha_\infty}$, where

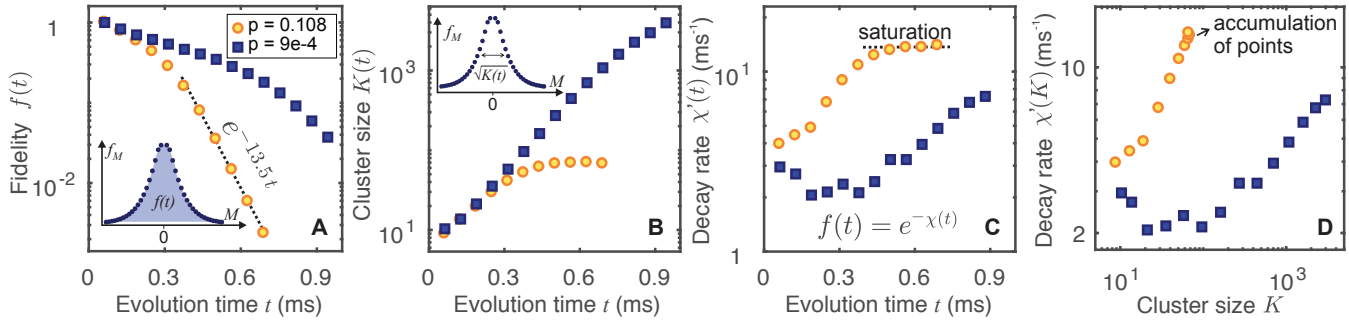

Figure 1. **Time evolution of the controlled-dynamics' fidelity and the corresponding effective cluster-size of correlated spins as a measure of the scrambling of information.** (**A**) The fidelity decay $f(t) = \langle I_z(t) I_z^0(t) \rangle$ is shown for two perturbation strengths, for the perturbation hamiltonian $\Sigma = \mathcal{H}_{dd}$. The strongest perturbation shows an exponential decay law for times > 0.3 ms. (inset) A MQC-fidelity $f_M(t)$ between the perturbed dynamic $I_z(t)$ and the ideal –non-perturbed– dynamics $I_z^0(t)$ as a function of the coherence order M. The enclosed area gives the global fidelity $f(t)$. (**B**) Evolution of the cluster-size of correlated spins $K(t)$ determined from the second moment of the MQC-fidelity (inset). The number of correlated spins $K(t)$ defines the "coherence length" on which the density matrices are comparable. For the weakest perturbations, the cluster size grows indefinitely, while for the strongest ones, $K(t)$ reaches a stationary value –an effect we call localization–. (**C**) The instantaneous decoherence rate $\chi'(p,t) = \frac{d\chi}{dt}(p,t)$ of the fidelity $f(t)$ as a function of time t. The exponential decay regimen of $f(t)$ is manifested here when the decoherence rate $\chi'(t)$ achieves a constant value. (**D**) The instantaneous decoherence rate χ' as a function of the cluster-size K. The plateau of $\chi'(t)$ that appears when the cluster size $K(t)$ localizes in (**C**), here is manifested by the accumulation of points at the end of the curve $\chi'(K)$.

$\alpha_\infty = 0.96 \pm 0.02$ for the perturbation $\mathcal{H}_{dd}$ and $\alpha_\infty = 0.79 \pm 0.03$ for $\mathcal{H}_z$, both near to a linear scaling. However, the exponents drop for the weakest perturbations as $p \to 0$. In the limit we obtain $\alpha_0 = 0.48 \pm 0.04$ for $\mathcal{H}_{dd}$ and $\alpha_0 = 0.47 \pm 0.02$ for $\mathcal{H}_z$ with the asymptotic behavior $\chi'(K) \sim K^{\alpha_0}$. This exponent is determined by the intrinsic decoherence effects that were not accounted in the quantum simulations (see Material and Methods).

To quantitatively analyze the different scaling laws determined by the exponent α on the different dynamical regimes for $K(t)$, we implement finite-time scaling techniques typically used to describe localization-delocalization transitions from finite-time experimental data [9, 31]. We consider the evolution time dependence implicit on the cluster-size $K(t)$. We use the single-parameter Ansatz for the scaling behavior at long times

$$\chi'(K,p) \sim K^{k_1} \Phi\left[\zeta(p_c - p) K^{-k_2 \nu}\right], \qquad (7)$$

consistently with previous experimental findings for the scaling law of the cluster-size growth $K(t)$ [9]. The constants k_1 and k_2 are determined to reproduce the asymptotic behavior at weak and strong perturbations. This assumption leads to the functional regimes $\chi' \sim (p_c - p)^s K^{\alpha_0}$ for $p < p_c$ and $\chi' \sim (p - p_c)^{-2\nu} K^{\alpha_\infty}$, for $p > p_c$ at long times (see Material and Methods). We determined the critical exponents from the asymptotic experimental data, obtaining $s = -0.986 \pm 0.002$ for $\Sigma = \mathcal{H}_{dd}$, $s = -0.46 \pm 0.02$ for $\Sigma = \mathcal{H}_z$ and $\nu = -0.56 \pm 0.01$ for both Σ. We then find the scaling factor $\zeta(p)$ that produces an universal scaling. Rescaled curves of χ' as a function of K that collapse into the universal scaling curve are shown in Fig. 3**A**,**B**. The two branches of the functional behavior, evidence two dynamical phases for the decoherence effect

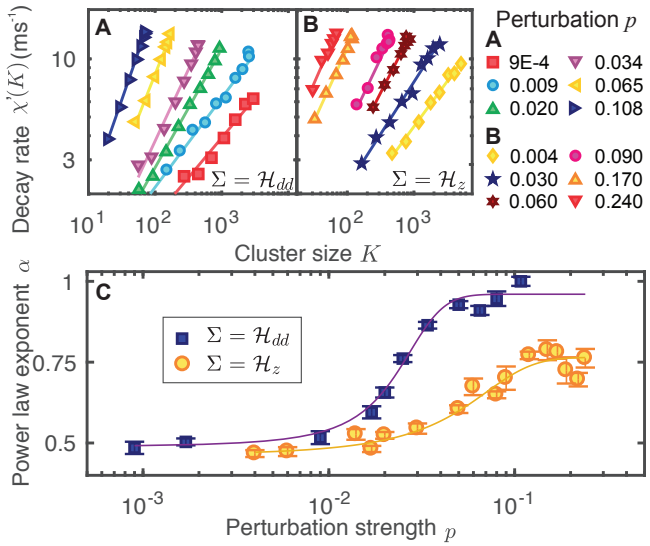

Figure 2. **Instantaneous decoherence rate χ' as a function of the effective cluster-size K.** The two perturbation Hamiltonians are considered (**A**) $\Sigma = \mathcal{H}_{dd}$ and (**B**) $\Sigma = H_z$. At long times, the fidelity decay rate is driven by the scrambling rate $\chi'(K) \sim K^\alpha$ given by the instantaneous cluster-size, with a power-law exponent that depends on the perturbation strength p. (**C**) The power law exponent α decreases with decreasing the perturbations strength, showing two plateau values at the weakest (α_0) and at strongest perturbation (α_∞).

on the controlled quantum operation characterized by the scrambling dynamics given by $K(t)$.

The scaling factors $\zeta(p)$ that lead to the universal scalings for both perturbations are consistent with the single

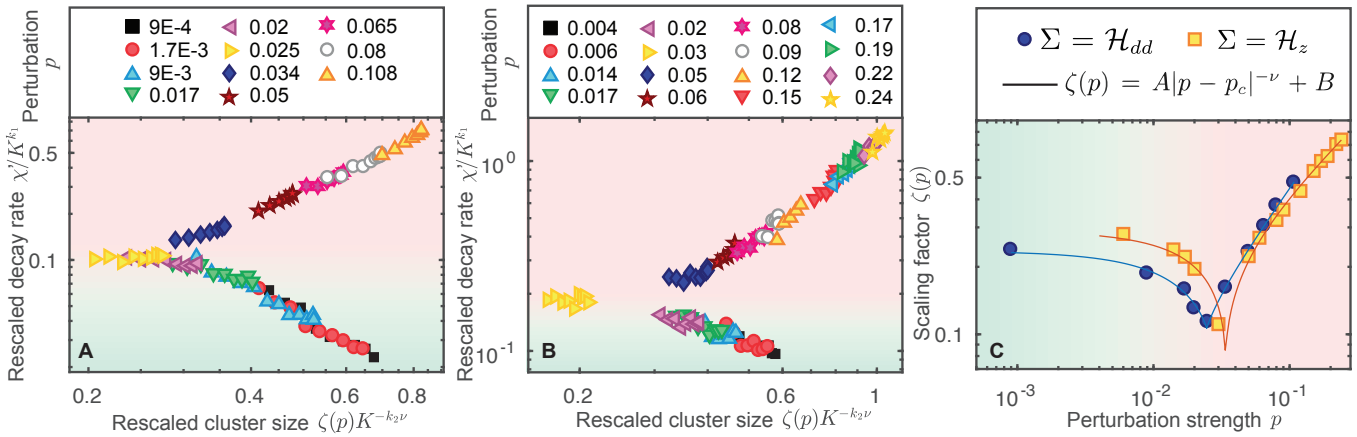

Figure 3. **Decoherence scaling transition between two dynamical regimes of the fidelity decay evidenced by the finite-time scaling analysis.** Scalings for both perturbation Hamiltonians (**A**) $\Sigma = \mathcal{H}_{dd}$ and (**B**) $\Sigma = \mathcal{H}_z$ are shown. (**C**) The corresponding scaling factors $\zeta(p)$ and their fittings to the function $\zeta(p) = A|p - p_c|^{-\nu} + B$. In the case of $\Sigma = \mathcal{H}_{dd}$, the critical exponents are $\nu = (-0.56 \pm 0.01)$ and $s = (-0.986 \pm 0.002)$ and critical perturbation $p_c = (0.024 \pm 0.04)$. For $\Sigma = \mathcal{H}_z$, the critical perturbation is $p_c = (0.034 \pm 0.01)$, and the critical exponents are $\nu = (-0.56 \pm 0.01)$ and $s = (-0.46 \pm 0.02)$. The curves of $\zeta(p)$ are normalized to satisfy $\zeta(p_\infty) = \sqrt{\chi'(K)/K^{\alpha_\infty}}$, where $p_\infty = 0.108$ for $\Sigma = \mathcal{H}_{dd}$ and $p_\infty = 0.24$ for $\Sigma = \mathcal{H}_z$ are the largest perturbation strength used in the experiments.

parameter ansatz of Eq. (7) that predicts a functional form $\zeta(p) \sim (p - p_c)^{-\nu}$ (Fig. 3**C**). The critical perturbation $p_c = (0.024 \pm 0.004)$ for $\Sigma = \mathcal{H}_{dd}$ is in agreement with previous experimental values that evidenced a localization-delocalization transition in the dynamics of the cluster-size $K(t)$ on the same system [9].

In summary, analyzing many-body Loschmidt Echoes we designed an experiment to measure an OTOC that quantifies the deviation of a perturbed dynamics from the ideal one based on monitoring the scrambling of information with MQC. We demonstrated that the fidelity decay rate of the ideal quantum information processing operation is driven by the instantaneous cluster-size $K(t)$ of correlated spins, which quantifies the information spreading induced by the control operation. The fidelity decay shows a transition between two different scaling laws that depends on the scrambling rate K^α, whose power law exponent changes suddenly as a function of the perturbation strength. By reducing the perturbation strength below a threshold, the exponent α drops abruptly below 1. This is encouraging as the dynamical decoherence rate does not scale linearly with the system size. Although the transition from one regime to another is smooth in the experimental data, due to the finite evolution time that is experimentally accessible, the finite-time scaling indicates the existence of the two dynamical regimes. The fact that the critical perturbation p_c is finite is also a promising feature for allowing reliable quantum control of large quantum systems if imperfections are below that threshold. The presented methods provide new avenues for controlling and characterizing many-body systems out-of-equilibrium for designing novel quantum technologies.

This work was supported by CNEA, ANPCyT-FONCyT PICT-2017-3447, PICT-2017-3699, PICT-2018-04333, PIP-CONICET (11220170100486CO), UNCUYO SIIP Tipo I 2019-C028, Instituto Balseiro. G.A.A. is member of the Research Career of CONICET. F.D.D. and M.C.R. acknowledges support from CONICET fellowships.

* federico.dominguez@cab.cnea.gov.ar
† Corresponding author: gonzalo.alvarez@cab.cnea.gov.ar

[1] J. Eisert, M. Friesdorf, and C. Gogolin, Nat. Phys. **11**, 124 (2015).
[2] D. A. Abanin, E. Altman, I. Bloch, and M. Serbyn, Rev. Mod. Phys. **91**, 021001 (2019).
[3] B. Swingle, Nat. Phys. **14**, 988 (2018).
[4] R. J. Lewis-Swan, A. Safavi-Naini, A. M. Kaufman, and A. M. Rey, Nat. Rev. Phys. **1**, 627 (2019).
[5] J. Zhang, G. Pagano, P. W. Hess, A. Kyprianidis, P. Becker, H. Kaplan, A. V. Gorshkov, Z.-X. Gong, and C. Monroe, Nature **551**, 601 (2017).
[6] H. Bernien, S. Schwartz, A. Keesling, H. Levine, A. Omran, H. Pichler, S. Choi, A. S. Zibrov, M. Endres, M. Greiner, V. Vuletić, and M. D. Lukin, Nature **551**, 579 (2017).
[7] C. Neill, P. Roushan, K. Kechedzhi, S. Boixo, S. V. Isakov, V. Smelyanskiy, A. Megrant, B. Chiaro, A. Dunsworth, K. Arya, R. Barends, B. Burkett, Y. Chen, Z. Chen, A. Fowler, B. Foxen, M. Giustina, R. Graff, E. Jeffrey, T. Huang, J. Kelly, P. Klimov, E. Lucero, J. Mutus, M. Neeley, C. Quintana, D. Sank, A. Vainsencher, J. Wenner, T. C. White, H. Neven, and J. M. Martinis, Science **360**, 195 (2018).
[8] H. G. Krojanski and D. Suter, Phys. Rev. Lett. **93**, 090501 (2004).
[9] G. A. Álvarez, D. Suter, and R. Kaiser, Science **349**, 846

(2015).
[10] D. Suter and G. A. Álvarez, Rev. Mod. Phys. **88**, 041001 (2016).
[11] S. Trotzky, Y.-A. Chen, A. Flesch, I. P. McCulloch, U. Schollwöck, J. Eisert, and I. Bloch, Nat. Phys. **8**, 325 (2012).
[12] K. A. Landsman, C. Figgatt, T. Schuster, N. M. Linke, B. Yoshida, N. Y. Yao, and C. Monroe, Nature **567**, 61 (2019).
[13] T. v. d. Sar, Z. H. Wang, M. S. Blok, H. Bernien, T. H. Taminiau, D. M. Toyli, D. A. Lidar, D. D. Awschalom, R. Hanson, and V. V. Dobrovitski, Nature **484**, 82 (2012).
[14] T. Schweigler, V. Kasper, S. Erne, I. Mazets, B. Rauer, F. Cataldini, T. Langen, T. Gasenzer, J. Berges, and J. Schmiedmayer, Nature **545**, 323 (2017).
[15] A. Lukin, M. Rispoli, R. Schittko, M. E. Tai, A. M. Kaufman, S. Choi, V. Khemani, J. Léonard, and M. Greiner, Science **364**, 256 (2019).
[16] T. Brydges, A. Elben, P. Jurcevic, B. Vermersch, C. Maier, B. P. Lanyon, P. Zoller, R. Blatt, and C. F. Roos, Science **364**, 260 (2019).
[17] I. Buluta and F. Nori, Science **326**, 108 (2009).
[18] I. M. Georgescu, S. Ashhab, and F. Nori, Rev. Mod. Phys. **86**, 153 (2014).
[19] J. Baum, M. Munowitz, A. Garroway, and A. Pines, J. Chem. Phys. **83**, 2015 (1985).
[20] M. Gärttner, J. G. Bohnet, A. Safavi-Naini, M. L. Wall, J. J. Bollinger, and A. M. Rey, Nat. Phys. **13**, 781 (2017).
[21] M. Gärttner, P. Hauke, and A. M. Rey, Phys. Rev. Lett. **120**, 040402 (2018).
[22] A. Peres, Phys. Rev. A **30**, 1610 (1984).
[23] H. M. Pastawski, P. R. Levstein, G. Usaj, J. Raya, and J. Hirschinger, Physica A **283**, 166 (2000).
[24] B. Yan, L. Cincio, and W. H. Zurek, Phys. Rev. Lett. **124**, 160603 (2020).
[25] J. Maldacena, S. H. Shenker, and D. Stanford, J. High Energy Phys. **2016**, 106 (2016).
[26] J. Li, R. Fan, H. Wang, B. Ye, B. Zeng, H. Zhai, X. Peng, and J. Du, Phys. Rev. X **7**, 031011 (2017).
[27] M. Niknam, L. F. Santos, and D. G. Cory, Phys. Rev. Research **2**, 013200 (2020).
[28] C. Sánchez, A. Chattah, K. Wei, L. Buljubasich, P. Cappellaro, and H. Pastawski, Phys. Rev. Lett. **124**, 030601 (2020).
[29] K. X. Wei, P. Peng, O. Shtanko, I. Marvian, S. Lloyd, C. Ramanathan, and P. Cappellaro, Phys. Rev. Lett. **123**, 090605 (2019).
[30] C. P. Slichter, *Principles of magnetic resonance*, Vol. 1 (Springer Science & Business Media, 2013).
[31] J. Chabé, G. Lemarié, B. Grémaud, D. Delande, P. Szriftgiser, and J. C. Garreau, Phys. Rev. Lett. **101**, 255702 (2008).
[32] W. Warren, S. Sinton, D. Weitekamp, and A. Pines, Phys. Rev. Lett. **43**, 1791 (1979).
[33] G. A. Álvarez and D. Suter, Phys. Rev. Lett. **104**, 230403 (2010).
[34] A. Kitaev and S. J. Suh, J. High Energ. Phys. **2018**, 183 (2018).
[35] A. Khitrin, Chem. Phys. Lett. **274**, 217 (1997).
[36] J. Baum and A. Pines, J. Am. Chem. Soc. **108**, 7447 (1986).
[37] U. Haeberlen and J. S. Waugh, Phys. Rev. **175**, 453 (1968).
[38] G. Lemarié, J. Chabé, P. Szriftgiser, J. C. Garreau, B. Grémaud, and D. Delande, Phys. Rev. A **80**, 043626 (2009).

MATERIALS AND METHODS

Hamiltonian engineering. The effective Hamiltonian of Eq. (3) is generated by concatenating short evolution periods $e^{-i\tau_0\mathcal{H}_0}$ and $e^{-i\tau_\Sigma\Sigma}$ of duration τ_0 and τ_Σ respectively. If the cycle time $\tau_c = \tau_0 + \tau_\Sigma \ll d^{-1}$, where $d \approx 13$kHz is the full-width-half-maximum of the resonance line determined by the homogeneous broadening induced by the dipolar coupling between the spins, we get $e^{-i\tau_0\mathcal{H}_0}e^{-\tau_\Sigma\Sigma} = e^{-i\tau_c[(1-p)\mathcal{H}_0+p\Sigma]+\mathcal{O}[(\tau_c d)^2]}$. Here $p = \tau_\Sigma/\tau_c$ is controlled by adjusting τ_Σ. Then based on the Suzuki-Trotter expansion, the evolution operator $U(t)$ is achieved by applying repetitively N cycles $e^{-i\tau_0\mathcal{H}_0}e^{-\tau_\Sigma\Sigma}$ of duration τ_c,

$$U(N\tau_c) = e^{-i[(1-p)\mathcal{H}_0+p\Sigma]N\tau_c}, \tag{8}$$

where the evolution time $t = N\tau_c$.

To engineer the double quantum hamiltonian $\mathcal{H}_0$, we use the 8-pulse sequence developed in Refs. [19, 32]. We applied $\pi/2$ RF pulses in the x direction of duration $\tau_p = 3.24\,\mu$s, with delays $\Delta = 2\,\mu$s and $\Delta' = 2\Delta + \tau_p$. The evolution operator of one cycle is

$$\begin{aligned} U(\tau_0) = e^{-i\Delta/2\mathcal{H}_{dd}}X^{-1}e^{-i\Delta'\mathcal{H}_{dd}}X^{-1}e^{-i\Delta\mathcal{H}_{dd}}X^{-1}\times \\ \times e^{-i\Delta'\mathcal{H}_{dd}}X^{-1}e^{-i\Delta\mathcal{H}_{dd}}Xe^{-i\Delta'\mathcal{H}_{dd}}Xe^{-i\Delta\mathcal{H}_{dd}}\times \\ \times Xe^{-i\Delta'\mathcal{H}_{dd}}Xe^{-i\Delta/2\mathcal{H}_{dd}}, \end{aligned}$$

where X is the $\pi/2$-pulse in the x direction. The duration of the pulse-sequence's cycle in our experiments was $\tau_0 = 62.88\,\mu$s. Again if $\tau_0 d \ll 1$, $U(\tau_0)$ approximates to

$$U(\tau_0) \sim e^{-\tau_0\mathcal{H}_0}. \tag{9}$$

The perturbation $\Sigma = \mathcal{H}_{dd}$ was prepared by a free-evolution period of duration τ_Σ following the cycle of $\mathcal{H}_0$ of duration τ_0 [9, 33]. The perturbation $\Sigma = \mathcal{H}_z = \Delta\omega_z I_z$ is produced by phase-shifts of the pulses that generate the $\mathcal{H}_0$ Hamiltonian by following the protocol proposed in Ref. [29]. The n-th cycle of the 8-pulse sequence that generates $\mathcal{H}_0$ is shifted by an angle $(n-1)\varphi$. Then, the evolution operator for the n-th cycle is

$$U_n(\tau_0) = e^{-iI_z(n-1)\varphi}\,e^{-i\mathcal{H}_0\tau_0}\,e^{iI_z(n-1)\varphi}, \tag{10}$$

and the concatenation of N cycles is then

$$\begin{aligned} U(N\,\tau_0) &= U_N \ldots U_1 && (11)\\ &= e^{-iN\varphi I_z}\left[e^{-i\tau_0\mathcal{H}_0}e^{i\varphi I_z}\right]^N \\ &= e^{-iN\varphi I_z}\left[e^{-i\tau_0\mathcal{H}_0}e^{i\tau_\Sigma d I_z}\right]^N && (12)\\ &\simeq e^{-iN\varphi I_z}e^{-i\tau_c N[(1-p)\mathcal{H}_0+p\Delta\omega_z I_z]}, && (13) \end{aligned}$$

where we have defined $\tau_\Sigma = \varphi/d$ and $\Delta\omega_z = -d$. As in the case $\Sigma = \mathcal{H}_{dd}$, $p = \tau_\Sigma/\tau_c$. The extra phase $e^{-iN\varphi I_z}$ is corrected by increasing the codification phase ϕ for determining the MQC spectrum in an angle $N\varphi$ [29]. The resulting effective Hamiltonian is then

$$\mathcal{H} \simeq (1-p)\mathcal{H}_0 + p\mathcal{H}_z. \tag{14}$$

Fidelity. We implement a Loschmidt Echo as a measure of the fidelity between the ideal density matrix evolving with $U_0(t) = e^{-it\mathcal{H}_0}$ and the perturbed one evolving with $U(t) = e^{-it\mathcal{H}}$. The resulting NMR signal is therefore $S(t) \propto \mathrm{tr}\left[U_0^\dagger U\rho(0)U^\dagger U_0 \cdot I_z\right] = \mathrm{tr}\left[UI_zU^\dagger U_0 I_z U_0^\dagger\right] = \mathrm{tr}\left[I_z(t)I_z^0(t)\right]$. We normalized the experimental data in Fig. 1**A** to obtain the fidelity $f(t) = S(t)/S(0) = \frac{\mathrm{tr}\left(I_z(t)I_z^0(t)\right)}{\mathrm{tr}(I_z^2)}$. To simplify notation we do not write the normalization factor.

Determination of the MQC-spectrum and the MQC-fidelity. The spin density matrix after evolving with the evolution operator $U(t)$ can be decomposed on coherence orders as

$$\rho(t) = \sum_M \sum_{m_j - m_i = M} \rho_{ij}(t)\,|m_i\rangle\langle m_j| = \sum_M \rho_M(t), \tag{15}$$

where the operator $\rho_M(t) = \sum_{m_j-m_i=M}\rho_{ij}(t)$ contains all the elements of the density operator involving the coherences of order M. Then a rotation $\phi_z = e^{-i\phi I_z}$ of a phase ϕ around the z-axis, changes the density operator to

$$\rho\,(\phi,t) = \phi_z\rho(t)\phi_z^{-1} = \sum_M e^{iM\phi}\rho_M(t). \tag{16}$$

The fidelity $f_\phi(t)$ with the proper normalization results then

$$\begin{aligned} f_\phi(t) &= \mathrm{tr}\left[\phi_z U\rho(0)U^\dagger\phi_z U_0 \cdot I_z U_0^\dagger\right] && (17)\\ &= \mathrm{tr}\left[\rho(\phi,t)\rho_0(t)\right] && (18)\\ &= \sum_{M'} e^{iM\phi}\mathrm{tr}\left[\rho_M(t)_M\rho_{0,M}(t)\right] && (19)\\ &= \sum_M e^{iM\phi}f_M, && (20) \end{aligned}$$

where $f_M(t) = \mathrm{tr}\left[\rho_{0M}(t)\rho_M(t)\right]$ is the MQC fidelity. The MQC-fidelity is therefore determined by performing a Fourier transform on ϕ of the echo signal $f_\phi(t)$. Similarly, when $p = 0$, $f_M^0(t) = \mathrm{tr}\left[\rho_{0M}(t)\rho_{0M}(t)\right]$ gives the MQC-spectrum [19].

OTOCs and the effective cluster-size $K(t)$. At $p = 0$, the fidelity $f_\phi^0(t) = \mathrm{tr}\left[\phi_z(t)I_z\phi_z^\dagger(t)I_z\right] = \left\langle\phi_z(t)I_z\phi_z^\dagger(t)I_z\right\rangle_{\beta=0}$ is a conventional OTOC, where $\langle\cdot\rangle_\beta = \mathrm{tr}(e^{-\beta\mathcal{H}}\ldots)/\mathrm{tr}(e^{-\beta\mathcal{H}})$ is the expectation value at the inverse temperature β [21, 25, 29, 34]. In our case the OTOC provides information of the system at infinite temperature with $\beta = 0$. In the main text we omit β to reduce

notation. The fidelity $f^0_\phi(t)$ quantifies the degree of non-commutation of $\phi_z(t)$ and I_z according to the relation

$$\left\langle [\phi_z(t), I_z]^\dagger [\phi_z(t), I_z] \right\rangle_{\beta=0} = 2 - 2f^0_\phi(t). \quad (21)$$

Performing a Taylor expansion of $f^0_\phi(t)$ for small ϕ, we get the second moment of the MQC-spectrum [21, 35]

$$m^0_2(t) = \sum_M M^2 f^0_M(t) = \left\langle [I_z(t), I_z]^\dagger [I_z(t), I_z] \right\rangle_{\beta=0}. \quad (22)$$

At $p = 0$, there are intrinsic decoherence effects that attenuates globally the $f^0_M(t)$ distribution (see "Intrinsic Decoherence effects" in Materials and Methods) as $f^0(t)$ decays as a function of time. Therefore the second moment of the MQC-spectrum $m^0_2(t)$ is normalized to the global fidelity $f^0_{\phi=0}(t)$ to remove the intrinsic decoherence effects allowing to quantify the width of the MQC-spectrum. This width is related to the number of correlated spins $K_0(t)$ [19, 36]. The exact value of K_0 will depend on the assumed model [35]. We use $K_0(t) = 2m^0_2(t)/f^0_{\phi=0}(t)$ assuming a Gaussian distribution for f^0_M [19]. $K_0(t)$ is determined from the width of a gaussian fit to obtain a more robust result compared to the one obtained directly using Eq. (22).

When $p \neq 0$, $f_\phi(t) = \left\langle I_z(t)\phi^\dagger_z I^0_z(t)\phi_z \right\rangle_{\beta=0}$ is a more general OTOC [34] that satisfies

$$\left\langle [I_z(t), \phi_z]^\dagger [I^0_z(t), \phi_z] \right\rangle_{\beta=0} = 2\left\langle I_z(t) I^0_z(t) \right\rangle_{\beta=0} - 2f_\phi(t) \quad (23)$$

$$= 2f_{\phi=0}(t) - 2f_\phi(t), \quad (24)$$

or expanding $f_\phi(t)$ in powers of ϕ, equivalently as done to obtain Eq. (22), we obtain the second moment

$$m_2(t) = \sum_M M^2 f_M(t) = \left\langle [I_z(t), I_z][I^0_z(t), I_z]^\dagger \right\rangle_{\beta=0}. \quad (25)$$

The second moment $m_2(t)$ quantifies the overlap between the scrambling of the ideal evolution $I^0_z(t)$ and the perturbed evolution $I_z(t)$. In analogy with the case $p = 0$, we normalize m_2 with the fidelity $f_{\phi=0}(t)$ to obtain an effective number of correlated spins $K(t) = 2m_2(t)/f_{\phi=0}(t)$.

Intrinsic Decoherence effects. The ideal form of the effective Hamiltonian $\mathcal{H}_0$ of Eq. (2) is based on an 0-th order approximation from average Hamiltonian theory [37]. It can only be achieved if the dipolar couplings d_{ij} are time independent, all pulses of the NMR sequences are ideal and the condition $\tau_c = \tau_0 + \tau_\Sigma \ll d^{-1}$ is good enough. However, typically these couplings are time dependent due to thermal fluctuations, and the pulses are not ideal. In addition, there are non-secular terms neglected in Eq. (1), and they might also contribute to the quantum dynamics. All these effects introduce extra terms in the effective Hamiltonian $\mathcal{H}$ of Eq. (3) and $\mathcal{H}_0$ of Eq. (2). These extra terms produce decoherence effects on ms time scales during the quantum simulations, even for $p = 0$. These decoherence effects reduce the detected signal and the overall fidelity $f(t)$. Then also the MQC-spectrum is attenuated with an overall global factor. However, on this study, this decoherence effects do not cause localization of the scrambling dynamics on the time scale of our experiments when $p \to 0$ (see Fig. 2, black squares). When $p \neq 0$, we quantify the scrambling rate K from the second moment of Eq. (6) generated by $\mathcal{H}_0$ after a time-reversed evolution under $-\mathcal{H}_0$. This means that these clusters have survived the decoherence effects. Therefore, the non-equilibrium many-body dynamics observed by the OTOC of Eq. (6), thus reflects the coherent quantum dynamics generated by the engineered Hamiltonians. We notice that, the experimentally observed quantum dynamics occurs over times scales much shorter than the spin-lattice relaxation time, $T_1 \approx 1$ sec, so we also neglect the effect of thermalization with the lattice.

Finite-time scaling procedure. To implement the finite-time scaling technique [9, 31, 38], we used the asymptotic experimental data for $p \to 0$, that shows that $\chi'(p \to 0, K) \propto K^{\alpha_0}$ for long times. Then we assume that $\chi'(p_\infty, K) \propto K^{\alpha_\infty}$ is satisfied also for long times, using the data for the largest perturbation strengths $p_\infty = 0.108$ for $\Sigma = \mathcal{H}_{dd}$ and $p_\infty = 0.24$ for $\Sigma = \mathcal{H}_z$. If there is a transition from these two regimes at a perturbation p_c, then close to the transition one expects a power law dependence on $(p - p_c)$ for the decoherence rate [9, 31, 38]. We then consider the following asymptotic functional dependence at long times

$$\chi'(p, K) \sim \begin{cases} (p_c - p)^s K^{\alpha_0} & p < p_c \\ (p - p_c)^{-2\nu} K^{\alpha_\infty} & p > p_c, \end{cases} \quad (26)$$

where the time dependence is implicit on K.

We use the single-parameter Ansatz for the scaling behavior at long times in order to find the scaling of the curves of Fig. 2, consistently with previous experimental findings [9]

$$\chi'(K, p) \sim K^{k_1} F\left[(p_c - p)K^{k_2}\right]. \quad (27)$$

Here $F(x)$ is an arbitrary function. Based on the asymptotic behavior of the experimental data, if $p < p_c$, then $\chi' \sim (p_c - p)^s K^{\alpha_0}$, implying that $F(x) \sim x^s$ and

$$k_1 + sk_2 = \alpha_0. \quad (28)$$

Then for $p > p_c$, $\chi' \sim (p_c - p)^{-2\nu} K^{\alpha_\infty}$ implies $F(x) \sim (-x)^{-2\nu}$ and

$$k_1 - 2k_2\nu = \alpha_\infty. \quad (29)$$

We estimate p_c from Fig. 2**C** and we found that the experimental data satisfy these asymptotic limits for $p \leq 0.009$ and $p \geq 0.05$ for $\mathcal{H}_{dd}$, and for $p \leq 0.02$ and $p \geq 0.12$ for $\mathcal{H}_z$. We obtain $s = (-0.986 \pm 0.002)$ for $\mathcal{H}_{dd}$,

$s = (-0.46 \pm 0.02)$ for $\mathcal{H}_z$ and $\nu = (-0.56 \pm 0.01)$ for both perturbations.

The scaling hypothesis is then generalized to

$$\chi'(K,p) \sim K^{k_1}\Phi\left[\zeta(p)K^{-k_2\nu}\right] \tag{30}$$

for accounting for the intermediate time regimes, where $\Phi(x)$ and $\zeta(p)$ again are arbitrary functions. This equation is less restrictive than Eq. (27) but includes it. Using the obtained critical exponents, and the values of α_0 and α_∞ obtained from the asymptotic limits in Fig. 2**C**, we get $k_1 = 0.70 \pm 0.05$ and $k_2\nu = -0.13 \pm 0.02$ for $\Sigma = \mathcal{H}_{dd}$ and $k_1 = 0.57 \pm 0.07$ and $k_2\nu = -0.10 \pm 0.02$ for $\Sigma = \mathcal{H}_z$ from Eqs. (28) and (29). The scaling behavior is then found by a proper determination of $\zeta(p)$.

To find the scaling factor $\zeta(p)$, we plot the curves of $\frac{\chi'}{K^{k_1}}$ as a function of $K^{-k_2\nu}$, and shift them by with $\zeta(p)$ to overlap with each other for different values of p in such a way that they generate a single curve as in Fig. 3. A single curve is only obtained if the experimental data is consistent with the scaling assumptions. To assure the consistency of the scaling determination, according to Eqs. (7) and (30), then the scaling factor must satisfy

$$\zeta(p) \sim (p - p_c)^{-\nu}. \tag{31}$$

The curves of $\zeta(p)$ are normalized to satisfy $\zeta(p_\infty) = \sqrt{\chi'(K)/K^{\alpha_\infty}}$, for the largest perturbation strength used in the experiments $p_\infty = 0.108$ for $\Sigma = \mathcal{H}_{dd}$ and $p_\infty = 0.24$ for $\Sigma = \mathcal{H}_z$. We then fit the experimental data with the function $\zeta(p) = A|p - p_c|^{-\nu} + B$, where the parameter B accounts for the external decoherence process that smooth the transition [9, 31, 38]. We observed the consistency of the fitted curves and the extracted critical exponents with the assumed single-parameter Ansatz. The critical perturbations from these fittings are then $p_c = (0.024 \pm 0.04)$ and (0.034 ± 0.01) for $\mathcal{H}_{dd}$ and $\mathcal{H}_z$ respectively. These values are consistent with the ones estimated from Fig. 2**C**.